Polarizations and Differential Cross Sections for the Elastic Scattering of 40-MeV Protons from ^{12}C, ^{40}Ca, ^{58}Ni, ^{90}Zr, and ^{208}Pb†

L. N. BLUMBERG,* E. E. GROSS, A. VAN DER WOUDE,‡ A. ZUCKER, AND R. H. RASSEL
Oak Ridge National Laboratory, Oak Ridge, Tennessee
(Received 11 March 1966)

The differential cross section and the polarization from the elastic scattering of 40-MeV protons were measured for ^{12}C ^{40}Ca, ^{58}Ni, ^{90}Zr, and ^{208}Pb. The polarized proton beam was obtained in two ways: (a) by scattering hydrogen from 80-MeV α particles, which gave $(89\pm7)\%$ polarization at an intensity of 2×10^7 p/sec; and (b) by elastic scattering of protons from Ca, resulting in $(35\pm3)\%$ polarization and an intensity of 1.5×10^8 p/sec. A 32-NaI(Tl)-detector array was used to measure the scattering at 10° intervals simultaneously. In addition to the elastic-scattering and polarization measurements given above, we also obtained the differential cross section and polarization for inelastic scattering from the 4.43-MeV state in ^{12}C, and the differential cross sections alone for the 7.66- and 9.63-MeV states. Optical-model calculations were made in such a way that simultaneous fits to the polarization and the differential cross section were obtained. An 11-parameter "best fit" search was made on each target, as well as an "average geometry" search where the geometric parameters were fixed and only the depths of the potentials allowed to vary. From the optical-model calculations we conclude that (1) the radius of the spin-orbit potential is smaller than that for the real potential, (2) for nuclei heavier than Ca, surface absorption alone gives a poorer fit than a combination of volume and surface absorption, and (3) the increase in well depth with A indicates the presence of a nuclear symmetry term in the real potential.

I. INTRODUCTION

INVESTIGATION of elastic scattering and polarization of protons from various nuclei has been of great importance in the development of the nuclear optical model. There is, however, still a dearth of this kind of information in the medium-energy region,[1,2,3] i.e., above 20 MeV. We have, therefore, undertaken to investigate this subject, paying particular attention (1) to assure ourselves that no inelastic scattering confuses our elastic results, (2) that measurements of the differential cross section and polarization extend over as wide an angular region as possible, and (3) to measure as accurately as possible the absolute value of the differential cross section. The primary theoretical motivation for the experiment was the acquisition of optical-model parameters for a number of targets, and at an energy where these parameters are as yet incompletely known. We report in this paper the first of a series of such experiments which are now under way at the Oak Ridge Isochronous Cyclotron (ORIC)—a variable-energy cyclotron which can produce, among other ions, protons between 20 and 68 MeV, and α particles between 40 and 80 MeV.

Two methods of preparing a polarized proton beam were used to obtain the results which are reported in this paper. Originally,[4] we bombarded a hydrogen target with 80-MeV α particles and made use of the 40-MeV recoil protons at 25.5° lab. These protons were found to have a polarization of $89\pm7\%$, and were produced in copious enough quantities ($\sim2\times10^7$ p/sec) to be useful for the measurement of polarization. In the course of the measurement of polarization from various elements, we found that at 40 MeV the elastic scattering from Ca at 25° yields protons with $35\pm3\%$ polarization, and that the cross section is unusually high (235 mb/sr). More recent measurements, and in fact all our current experiments, utilize polarized protons from the scattering on calcium.

The differential cross sections were measured with the direct, unpolarized 40-MeV proton beam from the cyclotron at the same energy as the polarization measurements, and with the same targets. As a rule the polarization was measured at 5° intervals from 10° to about 120°, and the differential cross section at 2.5° intervals from 10° to 170°. Optical-model parameters were obtained by a simultaneous fit of the polarization and scattering results.

II. THE EXPERIMENT

The polarized-proton facility was recently described in considerable detail.[4] To make the present paper complete, however, we shall here repeat some of the principal points relating to the experimental arrangement and methods of obtaining data. In addition, we shall describe the experimental method for the measurement of the differential cross section, a measurement similar to the polarization measurement, but differing from it in a few important details.

A. Polarized Proton Beam Preparation

A polarized proton beam was produced in either of two ways: first by utilizing the recoil protons from α-p scattering, and second by the elastic scattering of

† Research sponsored by the U. S. Atomic Energy Commission under contract with the Union Carbide Corporation.
* Present address: Harvard University, Cambridge, Massachusetts.
‡ Present address: University of Groningen, Groningen, The Netherlands.
[1] M. K. Brussel and J. H. Williams, Phys. Rev. 114, 525 (1959).
[2] B. W. Ridley and J. F. Turner, Nucl. Phys. 58, 497 (1964).
[3] R. M. Craig, J. C. Dore, G. W. Greenless, J. S. Lilley, and J. Lowe, Nucl. Phys. 58, 515 (1964).
[4] L. N. Blumberg, E. E. Gross, A. van der Woude, and A. Zucker, Nucl. Instr. Methods 39, 125 (1966).

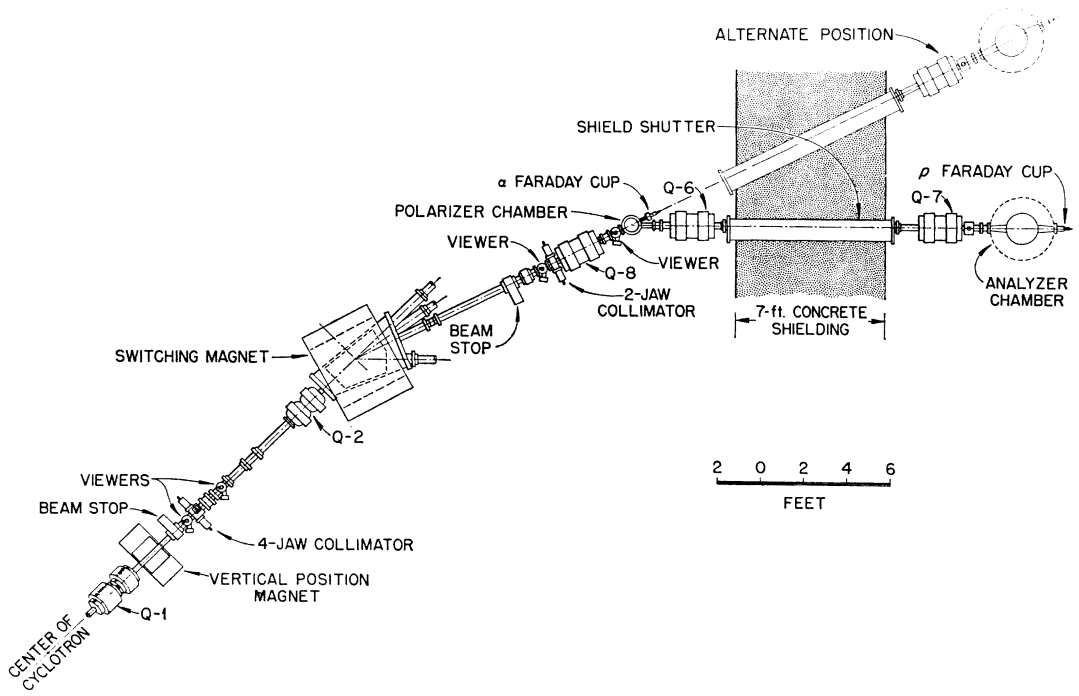

FIG. 1. Arrangement of beam optics for polarization measurements. The alternate position was used for cross section measurement in the direct cyclotron beam.

protons from Ca. In the first case the cyclotron beam of 80-MeV α particles was focused on a hydrogen-gas target operating at 120 psi pressure and at liquid-nitrogen temperature. Havar foils 0.0006 in. thick served as the entrance and exit windows for the beam, as well as the exit window for the polarized recoil protons. The incident α-particle beam was focused to a spot about 0.2 in. wide and 0.04 in. high on the hydrogen target. Polarized recoil protons at 25.5° to the incident beam were collected by a quadrupole lens and transported through a 7-ft concrete shield to the experimental room in which the scattering chamber was located. A second quadrupole lens focused the polarized beam to a narrow spot about 0.25 in. wide and 0.8 in. high. The general layout of the experiment is shown in Fig. 1.

For 1 μA of incident α particles we obtained 2×10^6 polarized protons per second, focused in the scattering chamber. Average beam conditions for the runs on which we here report resulted in about 8 μA of α particles and 1.6×10^7 protons/sec in the scattering chamber.

The polarized proton beam produced in this way has an energy spread of 1.4 MeV full width at half-maximum, (FWHM), due principally to the kinematic broadening which results from the horizontal angular acceptance of $\pm0.9°$ of the quadrupole beam transport system. This is a serious disadvantage, since it limits the measurement of polarization of elastic scattering to a small number of nuclei.

Our measurement of the polarization and differential cross section for the elastic scattering of 40-MeV protons from calcium revealed that this element would serve as an excellent polarizer. At 25.5° lab the polarization is -35.5% and the cross section 235 mb/sr. We, therefore, replaced the hydrogen gas cell by a 0.050-in. calcium foil, and bombarded it with 42-MeV protons. The calcium foil was about 2 MeV thick, and we thus obtained a 40-MeV polarized proton beam in the scattering chamber. With this Ca polarizer 1 μA of incident protons results in 1.25×10^7 polarized protons per second focused on the target. With a beam of 12 μA of protons incident on this target we have obtained, under the best conditions, 1.5×10^8 protons/sec focused on a spot 0.125 in. wide and 1 in. high in the scattering chamber. The energy spread of the elastic component of this beam was about 600 keV.

Besides the improvement in intensity, the calcium polarizer has several advantages over the (α,p) polarizer. It results in a smaller beam spot since the source is smaller. It produces less energy spread in the polarized beam. And finally, by virtue of the fact that 40-MeV protons are scattered in this arrangement, the background at the scattering chamber is much lower, and free of any unwanted particles which can produce 40-MeV pulses in the detectors. The disadvantages include the fact that inelastic scattering from calcium produces a beam at about 36.3 MeV which is also focused on the target, and which makes measurement of inelastic scattering of highly excited states impossible. The (α,p) beam has no inelastic component but reactions in the target windows give rise to a serious source of background. In principle the precision of a polariza-

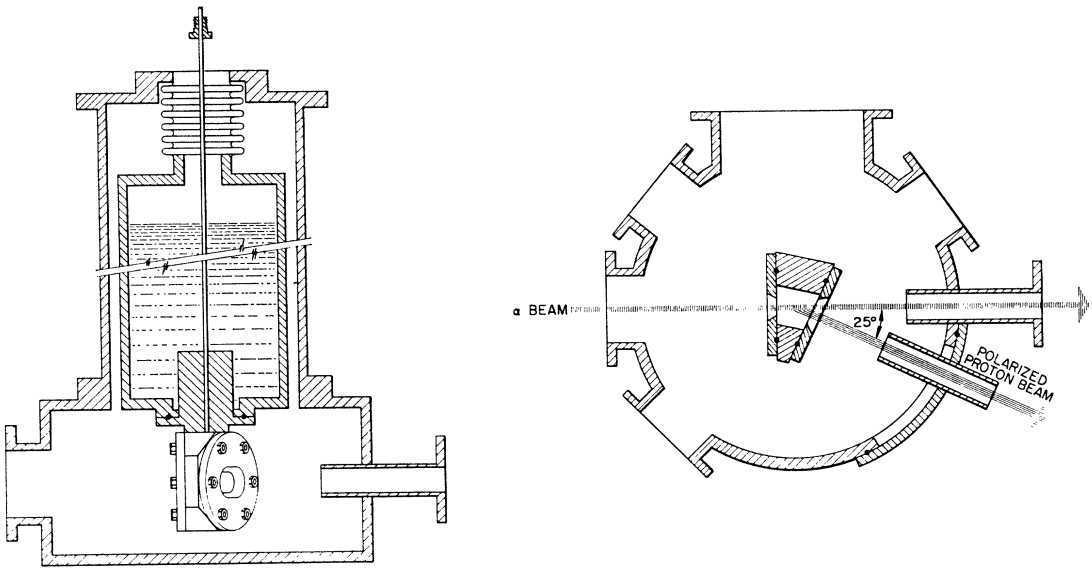

FIG. 2. Vertical and horizontal sections through the polarizer chamber showing the high-pressure H_2 target and its liquid nitrogen reservoir. When Ca is used as the polarizer, a 0.050-in.-thick water-cooled calcium disk replaces the hydrogen target and a primary proton beam replaces the α beam.

tion experiment is proportional to the product of the intensity and the square of the polarization of the incident beam, IP^2. In reality, however, uncertainties in background subtraction frequently introduce larger errors into the experiment than the statistical errors.

B. The Unpolarized Beam

A measurement of the polarization should also produce a differential cross section. Several difficulties, however, make the use of polarization data to construct differential cross sections impractical. First, it is difficult to measure the polarized beam intensity precisely, because of the plethora of charged particles, aside from the polarized protons, which are transmitted by the two quadrupoles. Also it is a simple matter, with our equipment, to measure the differential cross section at 2.5° intervals, from 10° to 170°. Polarization measurements of the same sort would have taken more time than was available. Lastly, the angular resolution of the detectors in the polarization measurement was ±2°; a value unnecessarily large for a precise determination of the differential cross section.

For all of these reasons a direct, unpolarized proton beam, with an energy spread <500 keV, and an angular divergence of <0.5° was focused at the center of our scattering chamber, but in a different location in the experiment room, shown as the "alternate position" in Fig. 1. The spot size was usually 0.125 in. wide and 0.250 in. high.

The direct beam was collected in a separately pumped graphite Faraday cup, the current amplified by an electrometer and integrated. The electrometer-integrator combination was calibrated and stable to about ±2%.

C. Targets

The targets which were bombarded in this investigation included ^{12}C, ^{40}Ca, ^{58}Ni, ^{90}Zr, and ^{208}Pb. Carbon and calcium were used in their natural isotopic abundance, while ^{58}Ni, ^{90}Zr, and ^{208}Pb were enriched to 99.95%, 97.8%, and 97.98%, respectively, in the desired isotope. The self-supporting metal targets were rolled to about 150 keV thickness for 40-MeV protons, the carbon target was a 50 mg/cm² thick machined piece of graphite. All targets were about ¾ in. wide and 2 in. tall.

Precise measurement of the thickness of the targets at the spot where the beam impinged proved to be a difficult matter. The material was too thick to allow measurement of the energy loss of 5-MeV α particles. We therefore prepared a separate set of thin targets whose thickness could be measured by the conventional method of determining the energy loss of 5-MeV α particles. In a separate experiment the thicknesses of the thin and thick targets were compared by measuring the yield of elastically scattered 40-MeV protons at a fixed angle. We found even the thin targets very inhomogeneous, and our value of the absolute differen-

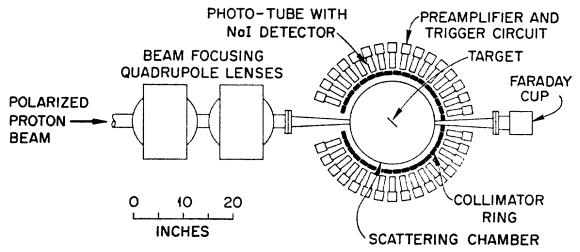

FIG. 3. Schematic diagram of the scattering chamber showing the 32-detector array and the collimator rings.

tial cross section is thus uncertain to $\pm 5\%$, due in part to the target inhomogeneity and in part to the uncertainty in the values of dE/dx for the low-energy α particles which were used.

Our targets were all sufficiently thin to resolve the elastic scattering from inelastic events, and yet as thick as possible to give a satisfactory counting rate when used with the weak polarized proton beam.

D. Scattering Chambers

Two scattering chambers were employed in this experiment. The first was fixed for an angle of 25.5° and served simply as a vacuum container for the hydrogen or calcium targets used to produce the polarized beam. It is shown in Fig. 2, with the hydrogen target in place.

The second chamber was the scattering chamber proper, in which the polarization and differential-cross-section measurements were carried out. It is shown schematically in Fig. 3. The chamber consists essentially of a 17-in. diameter vacuum envelope with a circumferential Mylar window which extends completely around the periphery except for two posts 1.5 in. wide at the extrnace and exit of the chamber. These posts support the vacuum load on the top of the chamber and also contain entrance and exit ports for the beam. Surrounding the window are two semicircular collimator holders with 16 slots in each, at 10° intervals. The collimator holders have slots which can be positioned so that the first aperture can be at any angle from 7.5° to 22.5°, and the successive 15 apertures follow at 10° intervals. Collimators with various apertures can be placed in the slots. For the polarization experiments the apertures were $\frac{3}{8}$ in. wide and $\frac{3}{4}$ in. high, and for the scattering experiments the apertures were circular, $\frac{1}{8}$ in. in diameter in all 32 positions. Behind each collimator is a NaI(Tl)-photomultiplier particle spectrometer, with a preamplifier and some address circuitry attached. The precision of the chamber is limited to the location of the beam entrance and exit ports, the target holder which is precisely centered, the collimator holders, the slots, and the collimators which fit in them. The solid angles subtended by all collimator apertures at the center of the chamber are equal to within $\pm 0.75\%$ and the maximum difference between any aperture on the left side and its partner on the right is 1%. We relied on the precision in the construction of the chamber to minimize instrumental asymmetry and considered it superfluous to provide a rotating mechanism by which the left and right sides of the chamber can be interchanged.

E. Electronics

The heart of the experiment lies in the thirty-two detector array, and a 20 000-channel analyzer used in conjunction with the detectors. The 20 000 channels are arranged into an assemblage of fifty 400-channel analyzers. Each of the photomultipliers is followed by a variable-gain preamplifier, and all preamplifiers in parallel are fed into one main amplifier in the counting room. Following each preamplifier is a Schmitt trigger circuit which feeds a pulse into a *BCD* matrix. Pulses from this matrix are used to set the address of the 20 000-channel analyzer. In this way we can collect data in 32 detectors simultaneously without using an excessive amount of electronics.

The detectors are 1-in.-diam, 0.29-in.-thick NaI(Tl) crystals mounted on selected RCA 6199 photomultipliers. To assure good resolution we accept detectors only if their resolution for the ^{137}Cs γ ray is better than 10% FWHM. Extrapolating this to 40-MeV protons, we expect counter resolutions ≤ 560 keV. In fact, we measured the resolution in all counters to be between 400 and 600 keV FWHM for 40-MeV protons.

The data from the 20 000-channel analyzer were read onto magnetic tape in a matter of seconds, and further processed by a digital computer, off line. The final data output is a machine-printed plot of the spectrum in each counter along with the number of counts in each channel, and the running sum of the counts of all channels up to the one in question. For clean peaks this last tabulation reduces the integration under a peak to the subtraction of two numbers.

F. Alignment

Careful alignment of the beam in the scattering chamber is essential to the success of a polarization measurement. The procedure we used was as follows. With beam entering the chamber through a window at the entrance port we placed 0.010-in. diameter cross hairs at the center of the chamber and exposed a Polaroid film immediately behind the cross hairs. By adjusting the position of the beam on the polarizer target with a bending magnet, the beam could be centered in the scattering chamber to within 0.016 in. For counters at small angles an error of 0.016 in. in beam centering introduces an error of 0.1° in left and right scattering angles. Next, we assume that scattering at 10° from ^{208}Pb is purely Coulomb, or at any rate that the polarization is very small. With the scattering chamber evacuated we placed a ^{208}Pb target at the center. The first counter in right bank was set at a nominal 10° and the left bank adjusted until the counting rate in its first counter was within 4% of the counting rate of its partner on the right. A 4% asymmetry would result from a 0.1° misalignment of the beam direction—the limit of our accuracy in beam spot positioning. Usually the left bank of counters had to be adjusted by 0.1° or less from its expected position.

Once the alignment was established it was checked with the ^{208}Pb target periodically during a run. It was found to be reliably stable, due principally to excellent current regulation of the bending magnet (1 part in 10^5) and of the quadrupole focusing magnets (Fig. 1).

Currents in all the beam transport elements were monitored at 1 h intervals during a run.

The alignment of the unpolarized beam was comparatively trivial, and required principally the establishment of the beam direction by counting on the left and right side of the beam.

G. Running Procedure

After the beam was aligned the polarization was measured by determining the left-right asymmetry of elastic scattering. Sufficient runs were taken to obtain data every 5° (lab) except in the case of ^{208}Pb where data were obtained every 2.5° because of the rapid fluctuation of polarization with angle, and in the case of ^{40}Ca where more angles were measured to investigate the polarization around 25°, after we decided to use this target as a polarizer. A separate series of runs, with the target tilted 45° to the incident beam was required to get data between 70° and 110°. Twelve hours of running time with 10^8 polarized protons/sec focused in the scattering chamber were usually required to measure the polarization from any one target from 10° to about 120°. In the course of each run the polarized beam was monitored with an ion chamber and a Faraday cup, but these were used only as indications for the length of a run, and no absolute reliability was demanded.

Measurements of the differential cross section differed from the polarization measurements in that the left and right banks of counters were placed at different angles with respect to the beam, so that data at 5° intervals could be obtained at one setting. Smaller collimators $\frac{1}{8}$ in. in diameter were used, and data were taken every 2.5°. Care had to be exercised that the dead time of the 20 000 channel analyzer did not introduce errors in the absolute value of the cross section. The dead time was measured in the following way. A scaler counted the Schmitt trigger pulses in all the odd counters, while another scaler was connected in such a way that it counted only those Schmitt trigger pulses from the odd counters which were accepted as address-setting signals by the 20 000 channel analyzer. The difference between the two scaler readings was proportional to the counts lost due to the dead time of the analyzer. Normally the beam intensity was regulated so that the dead time correction was less than 7%, and in the thin-target normalizing runs it was less than 1%.

It is clear that the most forward counters contribute by far the largest part of the counting rate, and that the beam intensity is limited by this fact. To obtain good statistics at back angles we placed lead absorbers in front of the first two counters on each side, thus blocking them completely. By this method it was possible to employ beams of several nA without incurring excessive dead time in the analyzer.

H. Measurement of the Beam Polarization

It is essential in this experiment to know the polarization of the incident proton beam. Since we were dealing with two proton beams, one produced as recoils from α-particle bombardment, and the other obtained from elastic scattering on Ca, we had to determine the polarization of each. The method chosen was to measure the polarization of the p-Ca beam by double scattering, and to relate the α-p beam polarization to it by an intermediate determination of the asymmetry of scattering from carbon at 60°.

Conceptually a double scattering experiment is very simple. One produces a beam by a first scattering, at a given angle and energy with a polarization P. If the second scattering is at the same energy for the same target, and if the left-right asymetry ϵ is measured at the same angle as the first scattering, the beam polarization $P=\sqrt{\epsilon}$. In practice this method is more complicated because the two scattering events do not take place at the same c.m. energy, and because finite solid angles are involved at each scattering and the scattering cross section may be a very strong function of the angle.

Our measurement of double scattering from calcium followed essentially the same procedure as the polarization measurements already described. We measured several angles near 25° to get a clear picture of the dependence of the polarization on angle around this first minimum. The first scattering was 25.5°±0.9°, and the second at 25.5°±2.0° (here the ± stands for the limits of the acceptance angle and not for the error in the scattering angle which was accurate to less than 0.1°). The principal problem was due to the fact that the elastic-scattering cross section around 25° is strongly angle dependent. A misalignment of the beam by 0.1° results in an asymmetry of 4%. The principal source of error in the measurement of the beam polarization is due just to this alignment error. The energy question, that is the effect on the measurement of the fact that the two scatterings do not occur at the same c.m. energy, proved not to be troublesome. Optical-model calculations and our measurements[5] at 35.8, 40.0, and 45.5 MeV indicate that the polarization at 25.5° varies only slowly with energy, and by using a 0.8-MeV-thick first scatterer and a 0.15-MeV-thick second scatterer we are assured that this source of uncertainty is much smaller than the error due to the misalignment errors.

The result of our measurement is that the beam polarization of 40-MeV protons elastically scattered to the right from natural calcium at 25.5° is -0.355 ± 0.03.

The polarization of the α-p produced beam was determined by measuring the asymmetry of scattering from carbon at 60° for both the p-Ca beam and the α-p beam. By using a carbon target the ratio of asymmetries can be very accurately determined because both

[5] E. E. Gross, R. H. Bassel, L. N. Blumberg, A. van der Woude, and A. Zucker, Proceedings, International Symposium on Polarization Phenomena, 1965 (to be published).

TABLE I. Differential cross section and polarization for 40-MeV proton elastic scattering from ^{12}C.

$\theta_{c.m.}$ (deg)	$\frac{d\sigma}{d\Omega}(\theta_{c.m.})$ (mb/sr)	$\frac{\Delta d\sigma}{d\Omega}$ (%)	$P(\theta_{c.m.})$	ΔP (%)
10.87	857	2	+0.068	12
13.58	842	2		
16.29	784	2	+0.008	75
19.00	647	3		
21.71	533	2	−0.010	230
24.41	473	2		
27.11	385	2	−0.051	14
29.81	232	4		
32.50	177	2	−0.078	18
35.19	128	2		
37.87	87.5	2	−0.105	8
40.54	53.8	6		
43.21	34.4	4	+0.008	350
45.88	24.4	2		
48.53	17.3	2	+0.326	4
51.19	12.4	7		
53.83	11.8	3	+0.706	4
56.47	11.0	6		
59.09	10.6	2	+0.775	2
61.72	10.2	7		
64.33	10.1	2	+0.719	2
66.93	9.40	4		
69.53	8.60	2	+0.652	2
72.12	7.79	6		
74.69	6.91	3	+0.593	4
77.26	5.80	7		
79.82	4.64	3	+0.516	5
82.38	3.77	2		
84.92	2.89	3	+0.505	10
87.45	2.36	2		
89.97	1.96	2	+0.439	13
92.49	1.69	6		
94.99	1.27	4	+0.460	9
97.49	1.08	3		
99.97	0.94	2	+0.426	13
102.45	0.93	9		
104.91	0.73	3	+0.488	16
107.37	0.75	7		
109.82	0.63	3	+0.476	9
112.26	0.59	7		
114.68	0.54	4	+0.575	22
119.52	0.40	8	+0.501	14
121.92	0.42	3		
124.31	0.38	4	+0.497	18
126.70	0.33	7		
129.08	0.32	4	+0.329	12
131.45	0.27	5		
133.81	0.27	6	+0.217	58
136.17	0.22	6		
138.52	0.23	6	+0.003	467
140.86	0.23	13		
143.20	0.21	10	−0.321	28
145.53	0.21	28		
147.85	0.23	14	−0.069	129
150.17	0.18	8		
152.49	0.20	13		
154.80	0.14	17		
157.10	0.22	24		
159.40	0.17	38		
161.70	0.16	15		
164.00	0.05	50		
166.29	0.08	35		
168.58	0.07	32		

TABLE II. Differential cross section and polarization for 40-MeV inelastic proton scattering from the 4.433-MeV level in ^{12}C.

$\theta_{c.m.}$ (deg)	$\frac{d\sigma}{d\Omega}(\theta_{c.m.})$ (mb/sr)	$\frac{\Delta d\sigma}{d\Omega}$ (%)	$P(\theta_{c.m.})$	ΔP (%)
10.92	17.9	9	+0.088	90
13.65	15.8	7		
16.38	18.8	13	−0.001	10400
19.10	16.9	10		
21.82	15.3	4	−0.049	233
24.53	16.2	4		
27.25	18.2	17	−0.142	21
29.95	15.8	10		
32.66	15.3	2	−0.232	23
35.36	14.3	2		
38.05	14.6	17	−0.225	7
40.73	14.7	17		
43.42	11.3	3	−0.190	35
46.09	9.9	3		
48.76	9.3	18	−0.299	12
51.42	7.7	11		
54.07	6.0	3	−0.265	16
56.71	4.6	9		
59.35	4.0	5	−0.186	16
61.98	3.5	6		
64.60	2.6	4	−0.039	205
67.21	2.1	5		
69.81	1.93	3	+0.180	19
72.41	1.85	7		
74.99	1.57	3	+0.547	12
77.56	1.35	3		
80.13	1.32	3	+0.712	4
82.68	1.38	4		
85.23	1.05	6	+0.772	4
87.76	1.27	6		
90.29	0.97	5	+0.817	9
92.80	0.96	9		
95.31	0.80	6	+0.860	3
97.80	0.76	8		
100.28	0.60	5	+0.870	3
102.76	0.61	8		
105.22	0.45	5	+0.586	13
107.68	0.41	10		
110.12	0.34	12	+0.547	10
112.56	0.28	22		
114.98	0.27	12	+0.156	29
119.80			+0.143	66
122.20	0.23	9		
124.59	0.25	13	+0.346	12
126.97	0.33	16		
129.34	0.36	9	−0.262	17
131.70	0.36	9		
134.06	0.47	17	−0.298	20
136.40	0.47	17		
138.74	0.57	9	+0.059	110
141.07	0.56	27		
143.40	0.69	22		
145.72	0.68	30		
148.03	0.90	28		
152.64	0.58	9		
157.23	0.53	17		

the asymmetry and the differential cross section vary very little with angle around 60°; in fact, both functions are essentially flat. The ratio of the polarization for the two kinds of beams was measured to be 2.50. From this ratio and the p-Ca polarization measurement we determined that the polarization of the 40-MeV recoil protons at 25.5° right from 80-MeV α-particle bombardment of hydrogen was $+0.89\pm0.07$. This value agrees, within the limits of error, with the measurement of Conzett *et al.*[6]

[6] H. E. Conzett, H. S. Goldberg, E. Shield, R. J. Slobodrian, and S. Yamabe, Phys. Letters **11**, 68 (1964).

TABLE III. Differential cross section for 40-MeV inelastic proton scattering from the 7.656- and 9.63-MeV levels in ^{12}C.

7.656 Level			9.63 Level		
$\theta_{c.m.}$ (deg)	$\frac{d\sigma}{d\Omega}(\theta_{c.m.})$ (mb/sr)	$\frac{\Delta d\sigma}{d\Omega}$ (%)	$\theta_{c.m.}$ (deg)	$\frac{d\sigma}{d\Omega}(\theta_{c.m.})$ (mb/sr)	$\frac{\Delta d\sigma}{d\Omega}$ (%)
10.97	5.97	45	13.75	1.47	35
13.71	1.53	40	16.50	2.31	30
16.45	2.42	25	19.24	2.09	10
19.18	0.61	33	21.98	1.75	29
21.91	0.43	48	24.71	1.83	24
24.64	0.36	57	27.44	1.88	25
27.36	0.38	19	30.17	3.07	14
30.08	0.34	18	32.89	2.89	7
32.79	0.68	20	35.60	3.18	10
35.50	0.69	30	38.31	3.62	10
38.20	0.60	10	41.02	4.00	20
40.90	0.85	40	43.71	3.54	4
43.59	0.67	11	46.40	3.20	15
46.27	0.54	15	49.08	3.38	10
48.95	0.52	16	51.76	3.91	20
51.62	0.54	25	54.42	3.26	5
54.28	0.43	12	57.08	2.93	20
56.93	0.35	12	59.73	2.79	10
59.57	0.35	12	62.37	2.97	20
62.21	0.29	25	65.00	2.29	7
64.84	0.29	11	67.62	2.00	10
67.45	0.26	12	70.23	1.83	15
70.06	0.30	17	72.83	1.88	25
72.66	0.43	14	75.43	1.42	10
75.25	0.25	29	78.01	1.34	10
77.82	0.29	11	80.58	1.27	10
80.39	0.26	12	83.14	1.45	10
82.95	0.33	13	85.68	1.01	10
85.50	0.24	13	88.22	0.97	9
88.03	0.20	15	90.75	0.72	24
90.56	0.21	38	93.27	0.99	10
93.07	0.14	50	95.77	0.69	6
95.58	0.14	14	98.26	0.67	6
98.07	0.10	20	100.75	0.58	11
100.56	0.11	45	103.22	0.69	6
103.03	0.13	15	105.68	0.62	8
105.49	0.10	20	108.13	0.58	7
107.94	0.06	33	110.57	0.50	8
110.38	0.06	33			

TABLE IV. Differential cross section and polarization for 40-MeV proton elastic scattering from ^{40}Ca.

$\theta_{c.m.}$ (deg)	$\frac{d\sigma}{d\Omega}(\theta_{c.m.})$ (mb/sr)	$\frac{\Delta d\sigma}{d\Omega}$ (%)	$P(\theta_{c.m.})$	ΔP (%)
10.26	5216	2	+0.025	27
12.83	3627	2	−0.028	34
15.39	2570	2	−0.082	12
17.95	1496	2	−0.12	8
20.51	920	2	−0.21	5
23.08	531	2	−0.32	6
25.64	249	2	−0.37	8
28.19	87.2	2	−0.41	5
30.75	50.6	2	−0.16	30
33.31	54.9	2	+0.32	6
35.86	75.9	2	+0.34	3
38.42	90.1	2	+0.29	7
40.97	96.7	2	+0.26	8
43.52	92.0	3		
46.06	79.8	3	+0.083	7
48.61	56.9	3	+0.012	42
51.15	40.2	3	−0.020	24
53.69	29.2	3		
56.23	18.2	3	+0.027	18
58.77	11.2	3	+0.23	9
61.30	8.48	3	+0.45	7
63.83	7.66	3		
66.36	7.50	3	+0.80	6
71.41	7.15	3	+0.79	5
73.93	6.68	3	+0.58	5
76.45	6.07	4	+0.58	7
78.97	4.61	4	+0.45	6
81.48	3.71	4	+0.45	6
83.99	2.87	5	+0.31	9
86.50	2.20	5	+0.33	9
89.00	1.62	5	+0.36	11
91.50	1.34	5	+0.48	10
94.00	1.21	5	+0.62	10
96.50	1.05	5	+0.68	9
98.99	1.01	5	+0.72	8
101.48	0.914	6	+0.94	10
103.97	0.829	7		
106.45	0.750	9	+0.94	10
108.93	0.636	9	+0.92	11
111.41	0.471	9	+0.85	11
113.89	0.461	9		
116.36	0.375	9	+0.74	13
118.83	0.287	9		
121.30	0.237	5	+0.71	21
123.77	0.212	5		
126.23	0.183	5	+0.38	32
128.69	0.168	5		
131.15	0.151	5	+0.38	39
133.61	0.132	6		
136.06	0.127	6	+0.46	26
138.52	0.132	6		
140.97	0.139	6	+0.34	44
143.41	0.146	6		
145.86	0.146	6	+0.65	20
148.31	0.161	6		
150.75	0.183	6	+0.66	15
153.19	0.196	6		
155.63	0.195	6	+0.53	19
158.07	0.208	6		
160.51	0.191	6	+0.29	34
162.95	0.172	7		
165.39	0.130	7	+0.10	120
167.83	0.119	7		
170.26	0.086	7	+0.23	65

It should be pointed out that the asymmetry of protons scattered from carbon around 60° provides an accurate and simple measurement in this energy region. It might be worthwhile to adopt this asymmetry as a secondary standard, and to measure the polarization from carbon at 60° as precisely as possible with beams whose polarizations are very well known. The carbon standard has many virtues: the target is easy to make and the counting geometry is simply established; the polarization is high; and as was stated previously, neither the polarization nor the cross section varies appreciably with angle, thus minimizing alignment errors. In addition the ground state of carbon is well separated from the first excited state, placing minimal requirements on beam energy homogeneity and detector resolution.

III. RESULTS

The results of this experiment are given in Tables I–VII, both for the polarization and the differential cross section. As a by-product of this experiment we have also obtained the differential cross section for the inelastic scattering from the 4.43-, 7.66-, and 9.63-MeV states in ^{12}C, as well as the asymmetry in the inelastic scattering from the 4.43-MeV state.

TABLE V. Differential cross section and polarization for 40-MeV proton elastic scattering from ^{58}Ni.

$\theta_{c.m.}$ (deg)	$\frac{d\sigma}{d\Omega}(\theta_{c.m.})$ (mb/sr)	$\frac{\Delta d\sigma}{d\Omega}$ (%)	$P(\theta_{c.m.})$	ΔP (%)
10.18	7557	1	+0.052	8
12.72	4570	1		
15.27	2734	1	−0.104	5
17.81	1395	1		
20.36	675	1	−0.151	2
25.44	67.8	3	−0.532	2
27.98	23.0	3		
30.52	50.8	3	+0.498	2
33.06	96.2	3		
35.60	131	3	+0.212	3
38.13	134	3		
40.67	121	3	+0.066	9
43.20	96.4	5		
45.73	67.0	5	−0.169	5
48.27	37.9	5		
50.80	22.1	5	−0.100	14
53.32	14.0	5		
55.85	11.5	5	+0.477	4
58.38	13.0	5		
60.90	14.7	5	+0.726	2
63.42	15.4	5		
65.94	15.6	5	+0.493	3
68.46	13.1	5		
70.98	10.9	5	+0.349	6
73.49	8.26	5		
76.00	6.02	5	+0.143	17
78.51	4.06	5		
81.02	2.94	10	+0.351	10
83.53	2.61	10		
86.03	2.37	10	+0.691	5
88.54	2.32	10		
91.04	2.56	10	+0.965	4
93.54	2.46	10		
96.03	2.51	10	+0.842	5
98.53	1.99	10		
101.02	1.63	10	+0.820	6
103.51	1.32	10		
106.00	1.02	10	+0.659	10
108.49	0.69	10		
110.97	0.63	10	+0.327	27
113.46	0.44	10		
118.42	0.46	10	+0.494	19
123.37	0.54	15		
125.85	0.46	15	+0.644	13
128.32	0.46	15		
130.79	0.41	15	+0.837	12
133.26	0.31	15		
135.73	0.28	15	+0.742	15
138.20	0.25	15		
140.67	0.14	15	+0.821	19
143.13	0.13	15		
145.59	0.084	15		
148.06	0.11	15		
150.52	0.13	15	+0.401	48
152.98	0.13	15		
155.44	0.15	15	+0.249	55
157.90	0.21	15		
160.35	0.23	15	−0.111	134
167.72	0.23	15		
170.18	0.20	15		

TABLE VI. Differential cross sectiona and polarization for 40-MeV proton elastic scattering from ^{90}Zr.

$\theta_{c.m.}$ (deg)	$\frac{d\sigma}{d\Omega}(\theta_{c.m.})$ (mb/sr)	$\frac{\Delta d\sigma}{d\Omega}$ (%)	$P(\theta_{c.m.})$	ΔP (%)
10.12	15866	1	+0.008	175
12.64	8301	1		
15.17	3724	1	−0.094	31
17.70	1373	1		
20.23	404	1	−0.220	12
22.76	104	1		
25.28	86.8	1	+0.337	13
27.81	196	1		
30.33	276	1	+0.129	21
32.86	307	1		
35.38	251	1	−0.123	23
37.91	161	1		
40.43	85.0	3	−0.392	4
42.95	41.1	3		
45.47	15.9	3	−0.163	15
47.99	14.2	3		
50.51	24.5	3	+0.726	8
53.03	33.2	3		
55.55	38.3	3	+0.270	8
58.06	35.1	3		
60.58	27.3	3	+0.017	156
63.09	19.5	3		
65.61	11.7	3	−0.299	16
68.12	6.32	3		
70.63	4.39	3	+0.340	11
73.14	4.72	3		
75.65	5.42	3	+0.882	3
78.15	6.14	3		
80.66	6.59	3	+0.689	5
83.16	5.97	3		
85.67	4.98	3	+0.317	17
88.17	3.37	3		
90.67	2.50	4	+0.182	33
93.17	1.66	4		
95.67	1.31	4	+0.348	13
98.16	1.19	4		
100.66	1.39	4	+0.848	6
103.15	1.31	4		
105.65	1.46	4	+0.772	7
108.14	1.25	4		
110.63	1.15	4	+0.620	10
113.12	0.93	4		
115.61	0.72	4	+0.527	16
118.09	0.52	4		
120.58	0.42	4	+0.461	24
123.06	0.31	4		
125.55	0.31	4	+0.218	64
128.03	0.35	4		
130.51	0.38	7		
132.99	0.38	7		
135.47	0.41	7		
137.95	0.41	7		
140.43	0.35	7		
142.91	0.30	7		
145.38	0.20	7		
147.86	0.17	7		
150.33	0.16	7		
152.81	0.12	7		
155.28	0.15	7		
157.76	0.17	7		
160.23	0.25	7		
162.70	0.28	7		
165.17	0.34	7		
167.64	0.37	7		
170.12	0.42	7		

The polarization $P(\theta)$ is ascertained from the left-right asymmetry $\epsilon(\theta)$ and the incident-beam polarization P_B

$$P(\theta)=\epsilon(\theta)/P_B.$$

The spin of the incident protons is polarized in the up direction for both methods of polarization used in this investigation. Then, following the Basel convention,

$$\epsilon(\theta)=(L-R)/(L+R),$$

where L is the number of counts on the left, at the

TABLE VII. Differential cross section and polarization for 40-MeV proton elastic scattering from ^{208}Pb.

$\theta_{c.m.}$ (deg)	$\frac{d\sigma}{d\Omega}(\theta_{c.m.})$ (mb/sr)	$\Delta\frac{d\sigma}{d\Omega}$ (%)	$P(\theta_{c.m.})$	ΔP (%)
10.05	73714	1	0	...
12.56	30282	1	0	...
15.07	11132	1	+0.018	108
17.59	5193	1		
20.10	2745	1	+0.048	40
22.61	1856	1	+0.045	40
25.12	1237	1	−0.031	55
27.63	628	1		
30.14	336	1	−0.170	11
32.66	168	1	−0.172	12
35.17	95.1	1	+0.150	16
37.68	98.9	1		
40.19	124	1	+0.221	10
42.70	123	1	−0.006	350
45.20	98.9	1	−0.109	17
47.71	51.0	1		
50.22	20.4	2	−0.496	10
52.73	7.84	2	−0.223	10
55.24	8.82	2	+0.472	9
57.74	17.3	2		
60.25	23.7	2	+0.271	14
62.76	22.1	2	+0.008	400
65.26	16.7	2	−0.221	15
67.77	8.82	2		
70.27	3.83	2	−0.444	16
72.78	2.04	2	−0.207	20
75.28	2.70	3	+0.509	16
77.78	4.34	3		
80.29	5.26	3	+0.447	16
82.79	5.42	3	+0.168	24
85.29	5.01	3	−0.014	569
87.79	2.58	3		
90.29	1.45	3	−0.418	29
92.79	1.05	3	−0.375	30
95.29	0.845	3	+0.155	101
97.79	0.997	3		
100.29	1.29	3	+0.109	182
102.78	1.27	3	+0.110	200
105.28	1.19	3	+0.339	34
107.78	0.938	3		
110.27	0.672	4		
112.77	0.465	4	+0.361	55
115.26	0.387	4		
117.76	0.289	4		
120.25	0.354	4		
122.74	0.399	4		
125.24	0.424	4		
127.73	0.412	4		
130.22	0.343	4		
132.71	0.228	6		
135.20	0.108	6		
137.70	0.147	6		
140.19	0.156	6		
142.68	0.191	6		
145.16	0.224	6		
147.66	0.215	6		
150.14	0.213	6		
152.63	0.174	6		
155.12	0.143	6		
157.61	0.150	6		
160.10	0.135	6		
162.59	0.174	6		
165.07	0.253	6		
167.56	0.315	6		
170.05	0.330	6		

angle θ, and R the number of counts on the right at the same angle. The errors in L and R were individually ascertained, and include statistical errors and the error due to uncertainties in background subtraction. The latter was sometimes especially bothersome, and could introduce uncertainties as large as 10%. The error $\Delta\epsilon/\epsilon$ in the asymmetry is calculated from the errors in L and R by the formula

$$\frac{\Delta\epsilon(\theta)}{\epsilon(\theta)}=2\left\{\left[\frac{L\Delta R}{L^2-R^2}\right]^2+\left[\frac{R\Delta L}{L^2-R^2}\right]^2\right\}^{1/2}.$$

The errors in $P(\theta)$ listed in the tables do not include the error in the determination of the polarization P_B of the incident beam, or systematic errors due to instrumental asymmetries. The latter could be as large as 4% at 10°, but they rapidly diminish in importance as the angle increases.

The errors given in Tables I–VII for the elastic scattering differential cross section are again relative, and include all sources of error except the ±5% uncertainty in the absolute measurement of the target thickness. The apparatus described above lends itself very well to precise measurements of the differential cross section because it accumulates data at many angles simultaneously. This eliminates the need for long runs and many normalizations, during which changes in the beam properties, the transport system or other drifts in the apparatus can occur. Corrections in the differential cross section were made for the loss of counts from the elastic peak on account of reactions of the protons in the NaI(Tl) crystal.[7] Estimates of multiple scattering show that corrections for this effect were unnecessary.

The angular acceptance of the counters was ±1.2° for the polarization data and ±0.4° for the scattering data.

IV. COMPARISON WITH THE OPTICAL MODEL

The principal motivation for this experiment, as has been pointed out, was to determine optical-model parameters for the scattering of protons at 40 MeV. With the results of the experiments described in the last section now available, it was merely a question of how to fit optical-model calculations to them most effectively. An eleven-parameter optical potential was used:

$$V(r)=V_c-V_0\left(\frac{1}{e^x+1}\right)-i\left(W_0-4W_D\frac{d}{dx'}\right)\frac{1}{e^{x'}+1}+\left(\frac{\hbar}{m_\pi c}\right)^2(V_s+iW_s)\frac{1}{r}\frac{d}{dr}\left(\frac{1}{e^{x_s}+1}\right)\boldsymbol{\sigma}\cdot\mathbf{l}.$$

Here V_0 is the depth of the real potential, W_0 and W_D volume and surface absorption terms, respectively, V_s and W_s the real imaginary spin-orbit depths, and m_π the pion mass. Further,

$$x=(r-R)/a,\quad x'=(r-R')/a',\quad x_s=(r-r_s)/a_s,$$

[7] D. F. Measday, Nucl. Instr. Methods 34, 353 (1965).

with

$$R=r_0A^{1/3},\quad R'=r_0'A^{1/3},\quad R_s=r_sA^{1/3}.$$

In the last three definitions, R is the radius variously defined for the real potential, imaginary potential, and spin-orbit potential, in that order, while a, a', and a_s are the Woods-Saxon rounding parameters for the same potentials. Finally,

$$V_c=Ze^2/r,\quad r>R_c$$

$$=\frac{Ze^2}{2R_c}(3-r^2/R_c^2),\quad r\leq R_c$$

is the Coulomb interaction from a uniform charge distribution with

$$R_c=r_cA^{1/3}.$$

The fitting was done using the computer program HUNTER[8] which varies the parameters until the quantity

$$\chi^2=\chi_\sigma^2+\chi_\pi^2$$

is minimized. Here

$$\chi_\sigma^2=\sum_i\frac{|\sigma_{\text{theor}}(\theta_i)-\sigma_{\text{expt}}(\theta_i)|^2}{[\Delta\sigma(\theta_i)]^2}$$

and

$$\chi_\pi^2=\sum\frac{|P_{\text{theor}}(\theta_i)-P_{\text{expt}}(\theta_i)|^2}{\Delta P(\theta_i)}.$$

ΔP and $\Delta\sigma$ are the experimental errors in the polarization and differential cross section, respectively.

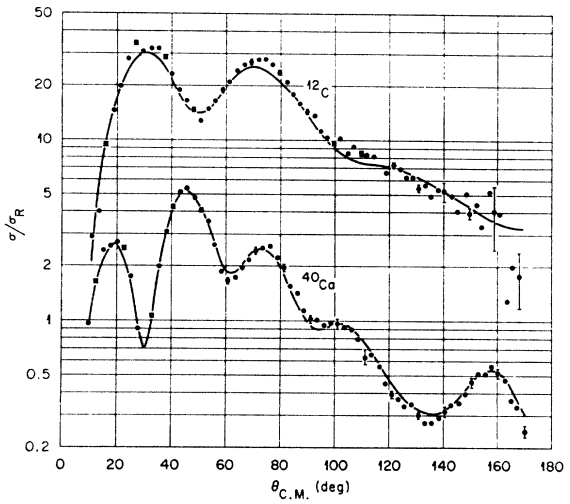

FIG. 4. Ratio-to-Rutherford differential cross sections for 40-MeV elastic proton scattering from ^{12}C and ^{40}Ca. Typical statistical error bars are shown. The solid curve represents the best fit obtained to the cross-section data if polarization data are ignored. The optical-model parameters are shown in Table VIII.

[8] R. M. Drisko (unpublished).

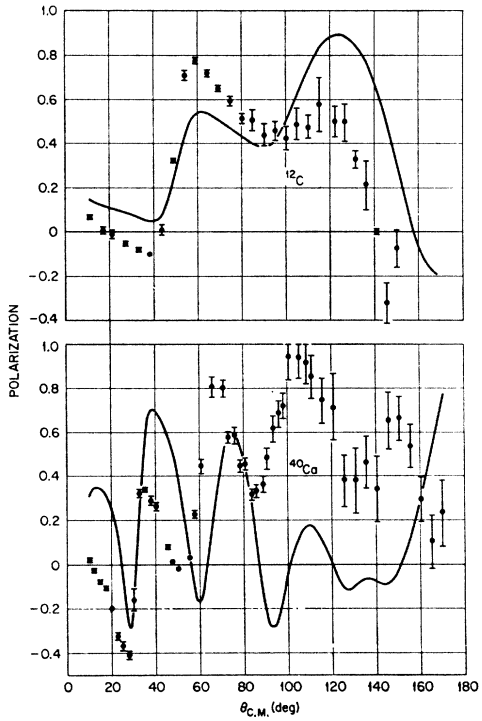

FIG. 5. Polarization versus center-of-mass angle for 40-MeV elastic proton scattering from ^{12}C and ^{40}Ca. Only statistical error bars are shown. The solid curve is the optical-model prediction corresponding to the differential cross section fits of Fig. 4.

A. "Optimum" Optical Potentials

All parameters were allowed to vary, within reasonable limits, until optimum (simultaneous) fits to the scattering and polarization data were found. As far as possible, the objective χ^2 test, discussed above, was used. This criterion often proved inadequate and a more subjective test in which the comparison of theory with data was judged pleasing to the eye was also used. It is important not to place too great an emphasis on minimizing χ^2, since in many cases this will result in forcing the fit at forward angles where the experimental errors are small at the expense of a general agreement between the data and the calculation. By general agreement we mean one which reproduces the major features of the cross section and polarization, e.g. position of extrema, slopes of the curves, etc. The subjective test was designed to get around the unquestioning faith in a minimum χ^2, especially in view of the fact that absolute normalization errors of $\pm5\%$ undoubtedly vitiate the simple χ^2 procedure.

The constraint of fitting both the scattering and polarization data was difficult to satisfy for the two lightest targets ^{12}C and ^{40}Ca. For either target it was possible to find good fits to the scattering as seen in Fig. 4, but the predicted polarizations bear little resemblance to experiment, Fig. 5. Alternatively, for ^{40}Ca, it was possible to fit the polarization but with a resultant poor fit to the scattering cross section, see

TABLE VIII. Optical parameters for ^{12}C and ^{40}Ca (as discussed in text).

	^{12}C (optimum σ)	^{40}Ca (optimum σ)	^{40}Ca (optimum P)
V_0 (MeV)	47.19	49.84	36.10
r_0 (F)	1.069	1.007	1.246
r_c (F)	1.250	1.250	1.250
a (F)	0.647	0.812	0.806
W_0 (MeV)	6.65	0	0
W_D (MeV)	0.328	6.20	3.69
r_0' (F)	1.354	1.097	1.331
a' (F)	0.731	0.805	0.665
V_s (MeV)	7.00	12.22	5.05
W_s (MeV)	0.00	0.01	0.41
r_s (F)	1.069	1.156	1.130
a_s (F)	0.647	0.830	0.649
χ_σ^2	110	101	3020
χ_π^2	5739	289 000	152
σ_R (mb)	37.8	83.0	68.6

Fig. 6. These results illustrate the necessity to consider both cross-section and polarization data when obtaining optical-model parameters. For ^{12}C we have not yet found a parameter combination which gives an adequate description of the polarization data.

The parameters found for the above cases are listed in Table VIII. For the remaining targets (^{58}Ni, ^{90}Zr, and ^{208}Pb) it was possible to find parameters which reasonably described both the polarization and scattering-cross-section data. These results, together with the best fits to ^{12}C and ^{40}Ca, are shown in Figs. 7 and 8,

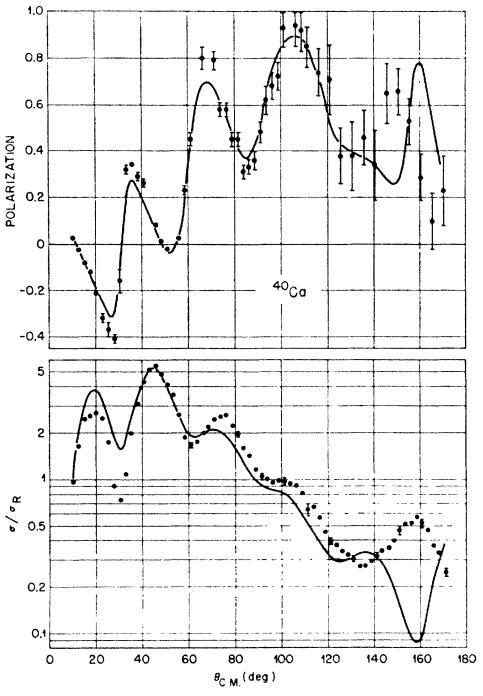

FIG. 6. Best fit to the ^{40}Ca polarization data is shown as the solid curve in the upper graph. The solid curve is the lower part of the figure is the corresponding prediction for the differential cross section for ^{40}Ca. The optical-model parameters are shown in Table VIII.

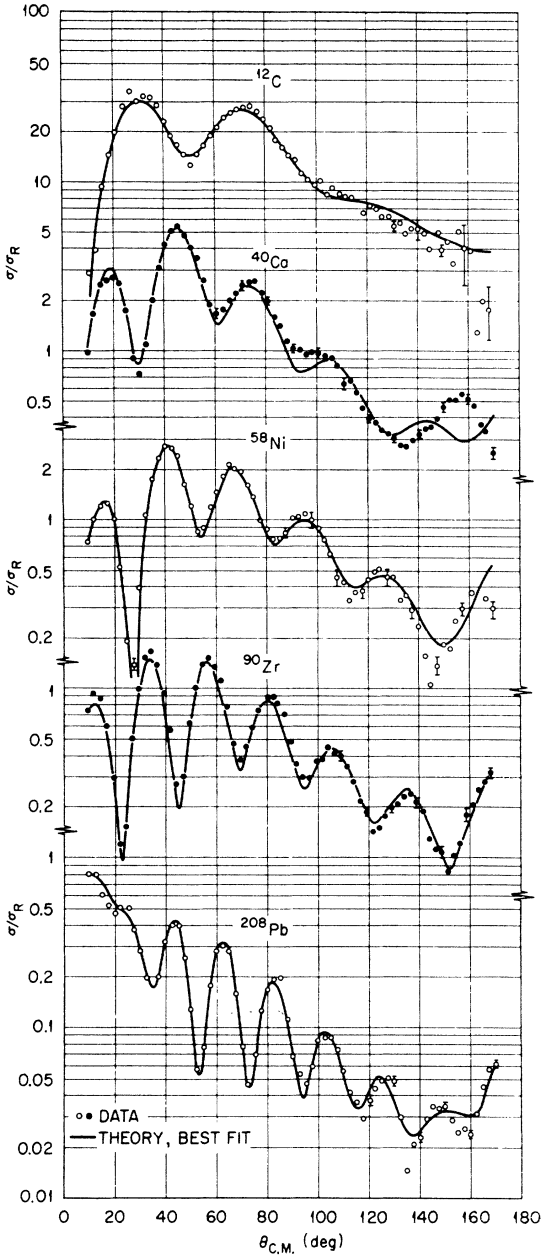

FIG. 7. Ratio-to-Rutherford differential cross sections for 40-MeV elastic proton scattering from ^{12}C, ^{40}Ca, ^{58}Ni, ^{90}Zr, and ^{208}Pb. Typical statistical error bars are shown. The solid curves represent the best simultaneous fits to the cross section and polarization data. Corresponding optical model parameters are shown in Table IX.

and the parameters listed in Table IX, along with the predicted reaction cross sections. Both χ_σ^2 and χ_π^2 are given for each target.

It is apparent that the optical parameters found from our best fits to ^{58}Ni, ^{90}Zr, and ^{208}Pb show certain similarities. In particular the radius parameter of the real well is in general less than 1.2 F and the diffusivity of the real well of order or greater than 0.7 F. Another general

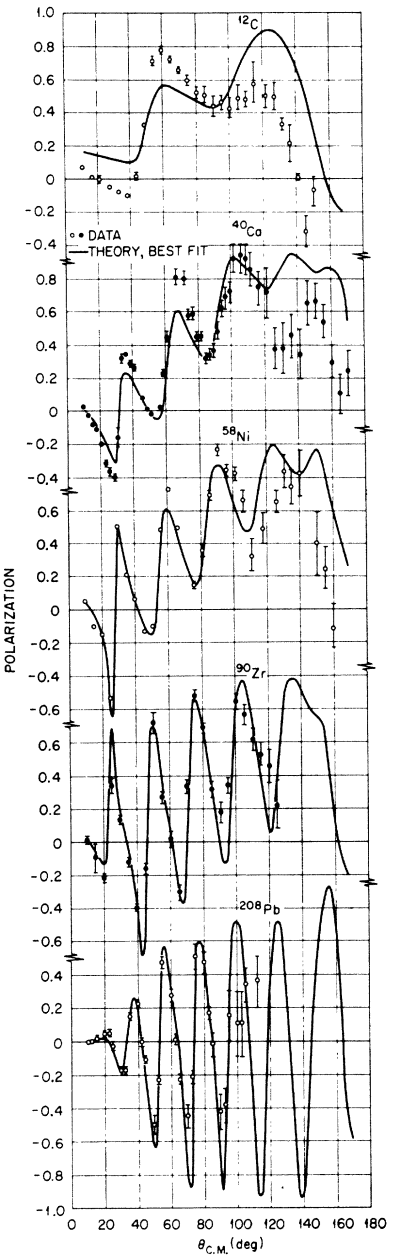

FIG. 8. Polarization versus center-of-mass angle for 40-MeV elastic proton scattering from ^{12}C, ^{40}Ca, ^{58}Ni, ^{90}Zr, and ^{208}Pb. Statistical error bars are shown. The solid curves represent the best simultaneous fits to the cross section and polarization data using the parameters of Table IX.

TABLE IX. Optical-model parameters from least-squares search of elastic-cross-section and polarization data which yielded minimum χ^2.

	^{12}C	^{40}Ca	^{58}Ni	^{90}Zr	^{208}Pb
V_0 (MeV)	47.20	40.15	45.91	46.51	53.49
r_0 (F)	1.070	1.229	1.158	1.178	1.150
r_c (F)	1.250	1.250	1.250	1.250	1.250
a (F)	0.650	0.689	0.721	0.678	0.803
W_0 (MeV)	6.60	0.00	7.34	4.66	2.00
W_D (MeV)	0.81	5.58	0.52	4.22	12.08
r_0' (F)	1.250	1.208	1.416	1.333	1.255
a' (F)	0.750	0.732	0.580	0.609	0.628
V_s (MeV)	7.00	3.92	5.67	6.59	5.62
W_s (MeV)	0.00	0.00	0.00	0.00	0.00
r_s (F)	1.100	1.080	1.047	1.027	1.136
a_s (F)	0.650	0.628	0.686	0.882	0.492
χ_σ^2	311	1022	424	1114	5737
χ_π^2	5268	854	822	682	257
σ_R (mb)	372	833	1040	1371	2044

feature of the parameters found for the "best" fits is that the imaginary part of the potential is a superposition of the Woods-Saxon shape ("volume" absorption) and the derivative of the Woods-Saxon shape ("surface" absorption), with the imaginary radius parameter greater than the real radius parameter and the diffusivity usually smaller than the diffusivity of the real well. Finally, the requirement of simultaneously fitting the polarization and cross section demanded that, within our parametrization of the model, the radius parameter of the spin-orbit interaction be taken smaller than the radius parameter of the real well, while the width parameter a_s is of the same order as the diffusivity a of the real well. This conclusion was reported earlier by us, and is supported by other evidence as well.[9–11] Finally, we note that the value of W_s, the imaginary spin-orbit potential was found to be zero or very small, for successful fitting of the data.

These results for the real well are in major agreement with the studies of Fricke and Satchler[12] who analyzed scattering data originating from the Minnesota group.[13,14] The geometrical parameters for the imaginary well, found in this study, are bounded by the parameters of Fricke and Satchler who considered the extreme "volume" or extreme "surface" shapes but not a mixture of the two types.

B. "Average" Optical Parameters

The results of our work discussed above indicated that the optical model was indeed capable of describing the data especially for the heavier nuclei. Since the best-fit parameters showed fluctuations from nucleus to nucleus, we decided that it was of interest to determine whether a fixed set of geometrical parameters could give an adequate description of the data. In this way, it was hoped that biases in the fitting procedure as well as uncertainties in the data and strict application of the model would be averaged out. The choice of an optimum set of geometrical parameters is difficult in view of the large number of parameters at our disposal. As a preliminary effort we chose these parameters as a rounded mean of the optimum parameters for the Ni, Zr, and Pb targets, with those for Zr weighted most

[9] L. N. Blumberg, R. H. Bassel, E. E. Gross, A. van der Woude, and A. Zucker, Bull. Am. Phys. Soc. 2, 103 (1965).
[10] D. A. Lind, D. E. Heagerty, and J. G. Kelly, Bull. Am. Phys. Soc. 2, 104 (1965).
[11] D. J. Baugh, J. A. R. Griffith, and S. Roman, in Proceedings International Symposium on Polarization Phenomena, 1965 (to be published).
[12] M. P. Fricke and G. R. Satchler, Phys. Rev. 139, B567 (1965).
[13] M. K. Brussel and J. H. Williams, Phys. Rev. 114, 525 (1959).
[14] T. Stovall and N. M. Hintz, Phys. Rev. 135, B330 (1964).

heavily. For the real well this led to a choice of parameters similar to those found by Fricke and Satchler ($r_0=1.18$ F and $a=0.7$ F). For the imaginary geometry $r_0'=1.3$ F and $a'=0.6$ F, while the spin-orbit radius and diffusivity parameters were taken as 1.05 F and 0.7 F, respectively. The depth of the spin-orbit well was fixed at 6 MeV. Variation of V_s between 5 and 7 MeV seems to have very little effect on the fit. An arbitrary choice of 6 MeV for this parameter then seemed appropriate.

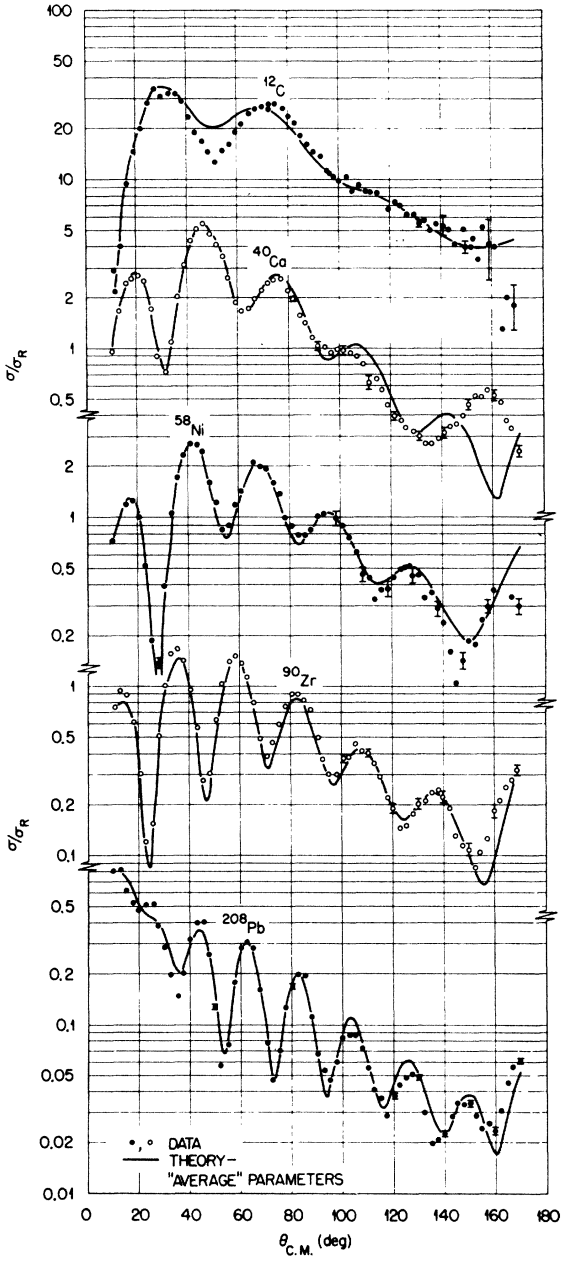

FIG. 9. Average parameter fits to the 40-MeV elastic proton scattering data. The solid curves result from a search on V_0, W_0, and W_D for a simultaneous fit to cross section and polarization data using the average parameters given in the text. The resulting values of V_0, W_0, and W_D are shown in Table X.

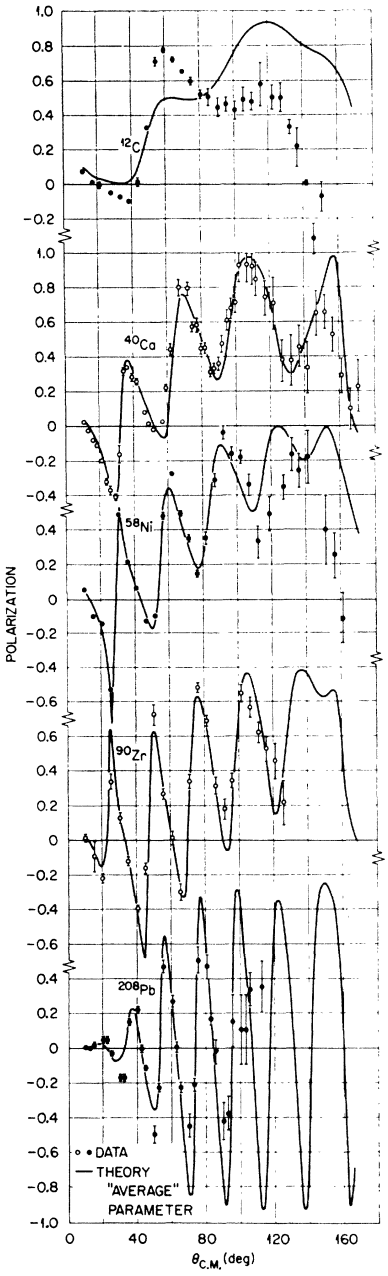

FIG. 10. Average parameter fits to the 40-MeV proton polarization data. The solid curves correspond to the cross section fits shown in Fig. 9.

With these parameters frozen, only the strengths of the real and imaginary central wells were allowed to vary as a function of target mass. For completeness the lighter nuclei (^{12}C and ^{40}Ca) were included in this survey. The results of these calculations are compared with the data in Figs. 9 and 10, while the central well strengths, reaction cross sections, and χ^2 values are listed in Table X. As can be seen in these figures, the fits to the scattering are quite good, indeed surprisingly so for the light nuclei. The polarizations also are well described except for ^{12}C.

Comparison of Figs. 7 and 9 reveals that the 11 parameter search is a better fit to large angle scattering

TABLE X. Central well strengths, reaction cross sections, and χ^2 values resulting from average parameter fits.

	^{12}C	^{40}Ca	^{58}Ni	^{90}Zr	^{208}Pb
V_0 (MeV)	38.8	43.3	44.7	47.3	52.7
W_0 (MeV)	4.8	2.0	7.1	4.8	7.5
W_D (MeV)	0.2	5.0	2.3	4.7	5.4
W_{max} (MeV)	4.8	6.1	6.6	7.4	8.7
χ_σ^2	1599	1114	486	1538	11361
χ_π^2	5294	1309	1090	368	293
σ_R (mb)	250	825	1045	1359	2007

from ^{40}Ca than the average parameter search, whereas the reverse is true for forward scattering. The glaring disagreement between theory and experiment for the (p, ^{40}Ca) elastic cross section near 160° is evidently a consequence of forcing the optical model to fit simultaneously cross-section and polarization data, since Fig. 4 reveals little difficulty in fitting the cross section data if the polarization data are ignored. This failure suggests the existence of another phenomenon not encompassed by the present formulation of the optical model. The difficulty in fitting ^{40}Ca data illustrates the danger inherent in relying solely on minimization of χ^2 in relating experimental results to optical-model calculations.

The general increase in well depth with increasing A can be associated, in the usual way,[15] with a dependence on the neutron excess of the target. Indeed if one takes the same Coulomb energy correction as Perey ($0.4Z/A^{1/3}$), our analysis yields the depth of the symmetry potential as 34.5 MeV. Since our analysis is applied to only three targets with nonvanishing neutron-excess parameter $(N-Z)/A$, we do not take the numerical value of the symmetry potential too seriously, but our results definitely indicate the presence of such a term.

The values of the coefficients of the volume and surface terms of the imaginary potential do not separately increase uniformly with target mass although their sum does. To put these numbers on the same footing we have computed the strength of the imaginary potential at its maximum for each target and have listed the results as W_{max} in Table X. This quantity is again a monotonic function of mass number, and, in fact, increases linearly with $A^{1/3}$.

[15] F. G. Perey, Phys. Rev. **131**, 745 (1963).

C. Conclusion

As can be seen in Figs. 9 and 10, our attempt to find an average optical potential to describe elastic scattering and polarization of 40-MeV protons has been moderately successful. In addition, the predicted reaction cross sections are compatible with available data at 30, 34, and 61 MeV.[16–18] For the light elements we have difficulties in describing the polarization data for ^{12}C and the back angle scattering from ^{40}Ca. For the heavier elements there are deficiencies in the fits to forward-angle scattering, a region where the optical model is assumed to be most applicable. This suggests that our average parameters, based on an analysis of essentially three targets, is in need of improvement. Measurement and analysis of elastic scattering and polarization data from six additional targets is in progress and it is expected that better average parameters should result from this analysis unless, of course, the idea of describing all nuclei with a fixed set of geometrical parameters is naive.

Our claim that the spin-orbit interaction is dissociated from the real central well rests mainly on describing the polarization at large angles for the Ni and Zr targets. There the requirement that the polarization be positive, coupled with an adequate representation of the scattering at these angles, forces the spin-orbit radius parameter to be small. This same set of conditions also requires that the imaginary well be a mixture of Saxon (volume) and derivative (surface) shapes.

ACKNOWLEDGMENTS

We take pleasure in acknowledging the support of R. S. Livingston and A. H. Snell in the course of this work, and many helpful discussions with R. M. Drisko and G. R. Satchler. We are indebted to W. H. White, A. W. Riikola, and the cyclotron operators, H. L. Dickerson, F. E. McDaniel, and C. L. Viar, for smooth operation of the cyclotron through many continuous hours of running, and to M. P. Fricke and B. J. Morton for their assistance during many of the runs and their help in the data analysis.

[16] J. F. Turner, B. W. Ridley, P. E. Cavanagh, G. A. Gard, and A. G. Hardacre, Nucl. Phys. **58**, 509 (1964).
[17] T. J. Gooding, Nucl. Phys. **12**, 241 (1959).
[18] V. Meyer, R. M. Eisberg, and R. F. Carlson, Phys. Rev. **117**, 1334 (1960).

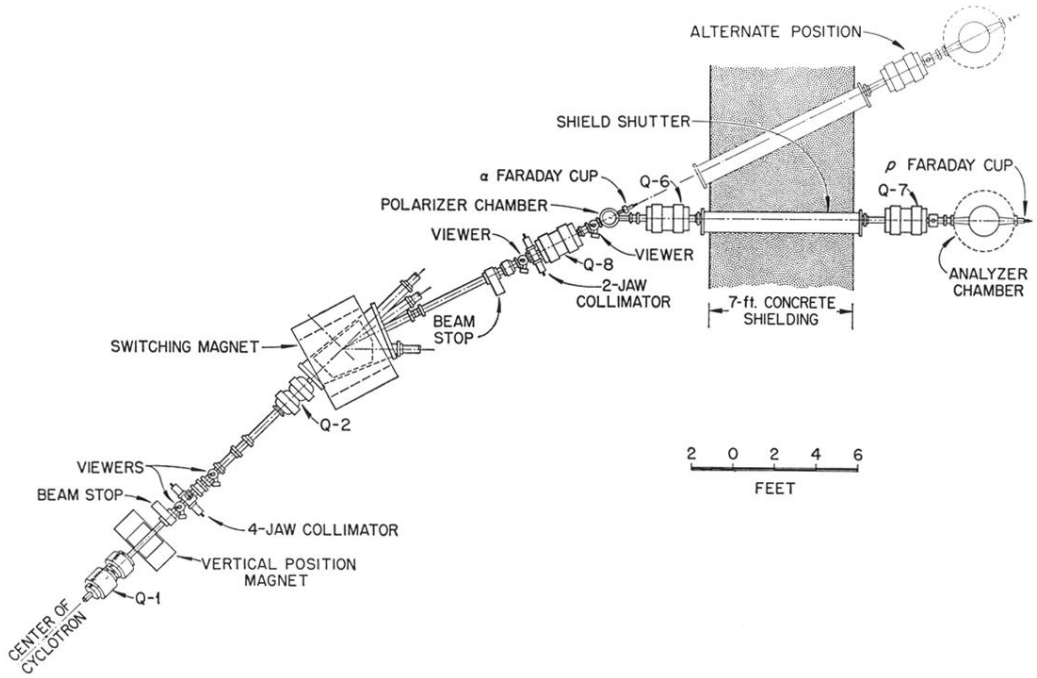

FIG. 1. Arrangement of beam optics for polarization measurements. The alternate position was used for cross section measurement in the direct cyclotron beam.